

A NEW LOOK AT TOP-OF-CANOPY GAP FRACTION MEASUREMENTS FROM HIGH-RESOLUTION AIRBORNE IMAGERY

Alemu Gonsamo and Petri Pellikka

University of Helsinki, Department of Geography, Helsinki, Finland; [alemu.gonsamo\(at\)helsinki.fi](mailto:alemu.gonsamo(at)helsinki.fi)

ABSTRACT

This study is aimed at demonstrating the feasibility of a large-scale leaf area index (*LAI*) inversion using high resolution airborne imagery without calibrating using ground based measurements. The study area is located in the Gatineau Park, Southern Quebec, Canada. The developed methods are evaluated in relatively high forest cover where remote sensing retrieval of biophysical parameters is commonly ill-posed. The airborne images were acquired on the cloud free day of August 21st, 2007 with 35 cm and 60 cm nominal pixel size of colour and colour infrared (*CIR*), respectively in digital format. The ground *LAI* measurements were collected from 54 plots of 20 m by 20 m using hemispherical photography between August 10th and 20th, 2007 and used as an evaluation dataset. *LAI* and other canopy structure parameters were computed from airborne imagery based on the principles commonly used for the ground based optical *LAI* estimation. A clumping index calculation algorithm is demonstrated using logarithmic gap fraction averaging technique based on the gap fraction data obtained from airborne imagery. The proposed methodology produced satisfactory results as related to the objective. The *LAI* inverted from *CIR* imagery (Pearson correlation coefficient with measured value $R = 0.67$) outperformed that of colour imagery. In view of that, such a methodology developed in this study could well be applicable particularly in low forest density areas and could further be improved.

INTRODUCTION

The major physiological processes of vegetation including photosynthesis and evapotranspiration are influenced by the vegetation biophysical parameters that describe the canopy structure. The quantification of canopy structure allows for knowledge of spatio-temporal dynamic processes occurring in the biosphere, in particular amongst vegetated land surfaces. Remote sensing provides the most feasible platform for spatially continuous observations of biophysical parameters for landscape to regional to global ecosystem studies in order to define realistic conditions of ecological models. Remotely sensed data offer a wide range of resolutions to estimate the biophysical parameters, although only recently does the increasing availability of high spectral, spatial and angular resolution provide better products. Leaf area index (*LAI*) is one of the principal biophysical parameters in climate, weather, and ecological studies, and has been routinely estimated from remote sensing measurements (1).

LAI is defined as one half the total leaf area per unit ground surface area projected on the local horizontal datum (2). The retrieval of *LAI* from remote sensing data is usually done based on empirical relationships between vegetation indices and ground based measurements. The problem with this approach is that it is affected by the noise of understorey and soil background reflectance and the saturation of vegetation indices at high *LAI* values (3). Another approach for canopy *LAI* retrieval is to invert a canopy reflectance model. However, there are no ideal canopy reflectance models that can be directly used for *LAI* inversion over large areas. Additionally, selection of the parameters for the inversion of canopy reflectance models is complicated, and some parameters are very difficult to determine. Generally speaking, the success of *LAI* estimation from remotely sensed data remains cumbersome and there is always a need to calibrate remotely retrieved parameters with ground based observation.

Remote sensing observations were also successfully used to derive vegetation fractional cover (*Fc*) from canopy radiance data. *Fc* is the percentage of vegetative cover projected vertically onto

ground. In the context of remotely-sensed images, the F_c values represent the percentage of vegetative cover present in each pixel or in a unit area such as the area equivalent of ground plots. A number of studies successfully estimated F_c aiming to relate with LAI from satellite remote sensing using the Normalized Difference Vegetation Index ($NDVI$) (4,5,6,7,8), spectral unmixing (9) and textural analysis (10). However, the use of satellite observations for F_c estimation is limited by the often coarse resolution of satellite observations, which results in mixed pixels made up of more than one land cover type. Furthermore, the accuracy depends on the size of the vegetation patches in relation to the pixel size. If the pixel size is too large compared to the vegetation patch, the F_c estimation relies on the mixed spectral response of canopy and surface, which is often a non-linear mix. By using high-resolution aerial imagery, relatively 'pure' small pixels of canopy, shadow and soil/litter can be obtained.

F_c derived from high-resolution airborne imagery is the complement of the mono-directional gap fraction. Gap fraction is the percentage of gaps in the canopy, meaning the chance of not hitting a leaf when casting a ray through a vegetation canopy. Gap fraction analysis is the most commonly used way of indirectly estimating LAI . Techniques based on gap fraction analysis assume that LAI can be calculated from canopy transmittance (the fraction of direct solar radiation which penetrates the canopy) and are well reported in the literature (e.g., 11). Measurements of canopy transmittance using optical field instruments are based on light recorded at a point under the canopy. This technique can also be applied by observing the canopy from above provided that high spatial resolution remote sensing imagery is available to distinguish gaps from canopy. From such a high-resolution gap fraction, LAI can be inverted using a simplified expression of light transmittance through a canopy, whereas the clumping index (CI) can be estimated based on the widely used logarithmic gap fraction averaging method (11). CI measures the deviation of foliage elements distribution from a spatially random manner. CI was reported to be the main factor causing errors in indirect LAI estimation (11). Model simulations have shown that the nadir remote sensing signal may be more related to the effective LAI , or the gap fraction, than to the true LAI (3), indicating the importance of CI .

This work is aimed at demonstrating the feasibility of methods for retrieving vegetation biophysical parameters without calibrating using ground based measurements. In this study, we developed large-scale inversion approaches to retrieve LAI , vegetation fractional cover (F_c) and clumping index (CI). The performance of the proposed approach was evaluated using ground measurements.

STUDY SITE AND DATA

Study site

The study site is located in the Great Lakes - St. Lawrence forest in Southern Quebec, Canada. It is part of the Gatineau Park (Figure 1), which is managed by the National Capital Commission (NCC) of Canada and centred at 45°30'N, 75°52'W. The park is about 10 km by 50 km and is mostly temperate hardwood forest with a dominant overstorey of sugar maple (*Acer saccharum* Marsh.) and small patches dominated by American beech (*Fagus grandifolia* Ehrh.), trembling aspen (*Populus tremuloides* Michx.), and red oak (*Quercus rubra* L.). Small numbers of red maple (*Acer rubrum* L.), American basswood (*Tilia americana* L.), ironwood (*Ostrya virginiana* (Mill.) K. Koch), white ash (*Fraxinus americana* L.), black ash (*Fraxinus nigra* Marsh.), white birch (*Betula papyrifera* Marsh.), and black cherry (*Prunus serotina* Ehrh.) are also present. The study plots were located in the southern portion of the park (Figure 1). They have been part of ongoing research on monitoring forest damage, structure, health and succession following the ice storm of 1998 (12). In 1998, 61 plots, each 20 m by 20 m, were placed on two north-south oriented transects in the Gatineau Park for the ice storm damage studies (12). Fifty-four of these plots that could be easily found in 2007 were selected. Plot corners were surveyed using differential GPS to provide positional accuracy on the order of <1 m. This level of accuracy is critical for airborne remote sensing where image pixel sizes are small.

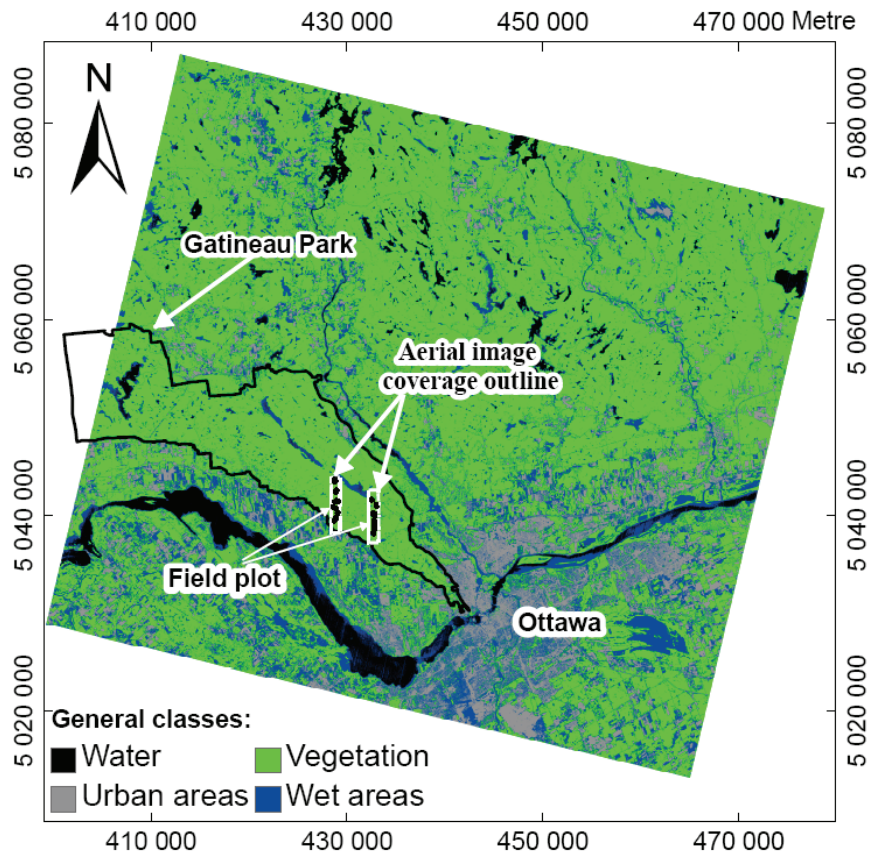


Figure 1: General land cover types derived from SPOT XS image taken on July 23, 2007 showing the Gatineau Park, outline of aerial image coverage and field plot locations of the study area. Projected coordinate system: NAD83 UTM Zone 18N.

Ground leaf area index measurements

The ground *LAI* measurements were collected using digital hemispherical photography between August 10th and 20th, 2007. The photographs were acquired using a high-resolution (8 mega pixels) Nikon Coolpix 8800 VR digital camera equipped with a fish-eye Nikon FC-E9 lens adapter (Nikon Inc., Japan). In total, five photographs were acquired in each study plot, one at each corner and one at the centre. The measurements were performed using recommended manual exposure under uniformly overcast conditions to minimize the anisotropy of the sky radiance and to reduce the scattering fluxes in the digital image. The camera was mounted and levelled on a tripod at a height of 1.3 m above ground. *LAI* was computed for the range of 0°-60° view zenith angle to reduce the increasing effects of mixed pixels near the horizon, which result from light scattering and coarse resolution. All photographs were analysed using CAN_EYE software (13). Fractional vegetation cover was extracted from the average gap fraction computed within 0°-20° view zenith angle as a compromise to represent a wider sampling area and the variability of *F_c*.

CAN_EYE computes *LAI* based on the use of a look-up-table derived using the Poisson model, i.e. a reference table composed of gap fraction value in different view zenith angles and the corresponding *LAI* and average leaf angle parameters using an ellipsoidal leaf inclination distribution. The ellipsoidal leaf inclination distribution assumes that the leaves are distributed parallel to an ellipsoid. The ellipsoidal distribution representing the special case of the spherical distribution which is widely used to describe the actual leaf inclination of many canopies makes the average leaf angle sufficient to characterize the leaf angle distribution function. The *LAI* value is computed assuming random foliage element distribution (clumping index: *Cl* = 1) and hereafter referred to as '*LAI* effective'. CAN_EYE also computes *Cl* using the logarithmic gap averaging technique (14) as:

$$Cl = \frac{\log \overline{P(\theta, \varphi)}}{\log P(\theta, \varphi)} \quad (1)$$

where $\overline{P(\theta, \varphi)}$ is the canopy mean gap fraction averaged from sky segments defined by zenith angle θ and azimuth angle φ and $\log P(\theta, \varphi)$ the logarithmic mean gap fractions of all segments. If the *LAI* is corrected for non random distribution of foliage elements based on the computed *CI* (Eq. 1), it is hereafter reported to as '*LAI* true'. If $CI = 1$, foliage elements are randomly distributed; $CI > 1$, foliage elements are regularly distributed (rare case, foliage elements are laid side by side); and $CI < 1$, foliage elements are clumped (common case, foliage elements are stacked on top of each other). In an effort to make all canopy variables estimated from hemispherical photography and airborne imagery comparable, we tried to follow the same parameter computation methods. In this regard, the *CI* shown in Eq. (1) is computed from the gap fraction extracted from segments where the Poisson law is more or less valid, i.e. the leaves are more or less randomly distributed. Therefore, in the cases of segments completely blocked with foliage elements, which does not allow the logarithmic calculation (Eq. 1), a new gap fraction is computed following the simple Poisson model by fixing *LAI* saturated value to 10 (explained later under the section of 'Large scale *LAI* inversion algorithms'). The summary of biophysical parameters obtained from ground measurements is given in Table 1.

Table 1: Summary of ground leaf area index measurements ($n=54$).

Variables	Mean	Minimum	Maximum	STDEV
<i>LAI</i> effective	4.03	2.60	5.70	0.66
<i>LAI</i> true	6.20	3.80	10.00	1.33
Clumping index	0.66	0.50	0.88	0.09
Fractional cover	0.88	0.64	0.99	0.07

Airborne imagery acquisition and processing

A data set of colour and colour infrared (*CIR*) digital camera images was captured on the cloud free day of the 21st of August 2007, between 12:32 and 13:24 local time, from an aircraft flying at approximately 309 m above ground level. During the acquisition, the solar zenith angle was between 34.3° and 33.6° and the azimuth angle was between 164° and 188.1°. The *CIR* camera was a Duncantech Multi-Spectral MS4100 with 1920 x 1080 pixel format and a 24mm lens. It is a 3-CCD camera with dispersion optics that splits the incident irradiance into three bands: green (500-600 nm), red (600-700 nm) and *NIR* (750-850 nm). The colour camera was a Nikon D200, having a single CCD with 3872 x 2592 pixel format and a 28 mm focal length lens. Exposures were set before each flight line to optimise the dynamic range and to result in image motion during each exposure of less than ½ a pixel. Exposure intervals for both cameras were set to provide 60% forward overlap. The nominal ground pixel size was 60 cm for the *CIR* data and 35 cm for the colour data.

The images were georectified using 25 cm pixel Orthophotos provided by the NCC. An average of 10 ground control points (GCPs) was selected for each image. A 1st-order polynomial and nearest neighbour interpolation were used as the warping and grey level resampling methods, respectively. The output projection for the registered images was UTM zone 18 with a NAD83 datum. Mosaics were assembled using pixels in the overlap area of each image pair that were closest to nadir. This minimized the effect of the bidirectional reflectance distribution function (BRDF), vignetting and light-fall off (15,16,17). The mosaics were also clipped from each side to restrict the across track view angle to 8°. The ground plots were distributed along the centre of the mosaic (flight line) so the between plot optical variation was minimised.

METHODS

To clarify the subsequent procedures described in this section, it is useful to recall the principle of the present study. We applied the *LAI* estimation algorithms developed for optical ground measurements where *LAI* is inverted from light transmission measurements recorded under the canopy. By assuming that the forest canopy is opaque, the only light transmission through the canopy is via

the gap. This gap, commonly called mono-directional gap fraction is the complement of fractional cover (F_c). Therefore, a prerequisite for LAI inversion is an accurate estimation of F_c and subsequently mono-directional gap fraction. We base our study on two approaches for gap fraction estimation one for each colour and CIR image. As a result, this section describes the approaches of LAI inversion for large scale study and also clumping index (CI) estimation from CIR image.

Fractional vegetation cover extraction from colour image

F_c from colour images was determined by visually setting red, green and blue threshold values to each image and calculating the ratio of canopy pixels to total pixel count in sub-scene of the image overlying on the ground plot from binary canopy-gap image. The threshold was extracted from thorough visual evaluation of the whole mosaicked area and was 7.8% for the red, 19.5% for the green and 31.3% for the blue band of the maximum dynamic range of the 8 bit image. Hence, the F_c is calculated as:

$$F_c = \frac{P_c}{P_t} \quad (2)$$

where P_c is the number of pixels recorded as canopy and P_t is the total number of pixels in a specific plot sub-scene.

Fractional vegetation cover extraction from CIR image

The Normalized Difference Vegetation Index ($NDVI$) is the most commonly used index for vegetation, fractional cover, LAI and other biophysical parameter studies (18,19). The most common method to estimate F_c from a vegetation index uses $NDVI$ (4,5,6,7,8,20). $NDVI$ is computed from reflectance of red and near infrared (NIR) spectral bands of the CIR image as:

$$\frac{NIR - RED}{NIR + RED} \quad (3)$$

$NDVI$ of a mixed pixel is a weighted sum of vegetation $NDVI$ ($NDVI_g$) and non-vegetation $NDVI$ ($NDVI_{back}$) (4,21,22):

$$NDVI = F_c NDVI_g + (1 - F_c) NDVI_{back} \quad (4)$$

Therefore, the F_c of a mixed pixel can be computed as:

$$F_c = \frac{NDVI - NDVI_{back}}{NDVI_g - NDVI_{back}} \quad (5)$$

where $NDVI_g$ is the maximum or saturated $NDVI$, which is defined as the $NDVI$ where vegetation occupies the full field of view, and $NDVI_{back}$ is the minimum or background $NDVI$. To determine the saturated and background $NDVI$, the CIR image mosaics were first classified into water, built-up areas and vegetated areas including open agricultural fields. Then the mask was developed containing vegetated area and non-vegetated area (water and build-up areas). The $NDVI$ is computed for the vegetated area and open field, and the histogram was drawn by combining the $NDVI$ from both transect mosaics. The $NDVI$ values at the lower and upper end of 1% cut-off bounds (1st and 99th percentiles) in the histogram were taken as background and saturated $NDVI$ values, respectively. Other studies have used 90th percentile as $NDVI_g$ because $NDVI$ increases with increasing view angle due to the effect of multiple scattering (7). However, in this study, with narrow view angle and high spatial resolution, the 99th percentile was deemed to be reliable in representing saturated $NDVI$. The background and saturated $NDVI$ computed from the 1% cut-off bounds were 0.0412 and 0.796, respectively. The background $NDVI$ is within a range of what is found by other studies 0.02-0.05 (4,7,21,22). As illustrated in the following section, the background $NDVI$ has little influence on the accuracy of LAI inversion.

As demonstrated in Eq. (5), $NDVI$ can be either less or greater than $NDVI_{back}$ and $NDVI_g$, respectively due to the 1 % cut-off bounds of the actual $NDVI$ range. Consequently, F_c computed can be negative or greater than 1. In negative cases, the computed F_c is forced to 0 and in the cases of greater than 1, F_c is forced to 1.

Large scale LAI inversion algorithms

Light extinction models describe the probability of interception of radiation within canopy layers, as well as the probability of sun flecks at the bottom of the canopy corresponding to gaps in the canopy when viewed along the direction of the direct solar beam. As described earlier, assuming that the tree crowns are opaque and the only transmission is through the gaps in the canopy, the fraction of incident light transmitted through a canopy or mono-directional gap fraction (P_o) can be described as:

$$P_o = 1 - Fc \tag{6}$$

P_o can be related to LAI using Lambert-Beer's law as (24):

$$P_o = \exp(-kLAI) = 1 - Fc \tag{7}$$

Therefore, for a known value of P_o and k , LAI can be calculated as:

$$LAI = \frac{-\ln P_o}{k} = \frac{-\ln(1 - Fc)}{k} = \frac{-\ln(1 - P_c/P_t)}{k}$$

$$\text{or: } \frac{-\ln \left[1 - \left(\frac{NDVI - NDVI_{back}}{NDVI_g - NDVI_{back}} \right) \right]}{k} \tag{8}$$

where k is an extinction coefficient. For a broadleaved forest, k typically ranges between 0.42-0.58 (23; see summary of lists of different values). In this study, k was assumed to be 0.5, which is a good approximation for a broadleaved forest considering the near nadir view.

For segments with no gap, 'empty segments', those with $P_o = 0$ not allowing the calculation of logarithm, a new value of gap > 0 is computed using a local Poisson model:

$$P(o) = \exp(-0.5LAI/sat) \tag{9}$$

where LAI/sat is maximum (saturated) LAI forced to a prescribed value of 10 (13).

The clumping index (CI) from CIR mosaic derived NDVI is calculated in the same manner as applied in CAN_EYE (Eq. 1) using the logarithmic gap averaging technique (14) as:

$$CI = \frac{\text{LOG} \left[1 - \left(\frac{NDVI - NDVI_{back}}{NDVI_g - NDVI_{back}} \right) \right]}{\text{LOG} \left[1 - \left(\frac{NDVI - NDVI_{back}}{NDVI_g - NDVI_{back}} \right) \right]} \tag{10}$$

The 'empty segments' where vegetation is full field of view, new gap fraction is calculated using a local Poisson model (Eq. 9). The CI is used to correct the computed LAI effective from CIR mosaics into LAI true. Both LAI and CI are computed from approximately 1111 pixels which is equivalent to the ground plot size. In subsequent LAI mapping from the whole mosaic image with the best of the two gap fraction extraction algorithms, 20 m by 20 m grid in a north-south orientation (the same as the ground plot orientation) can be used and the gap fraction can be computed and inverted for each cell.

RESULTS

The main assumption of LAI inversion particularly from colour images was that the complement of Fc equals the gap fraction. To demonstrate the sensitivity of Fc to forest density, we first evaluated the relationship between the measured and estimated Fc from the colour imagery. As commonly noted, the correlation between Fc measured using hemispherical photography and estimated using remotely sensed observations are typically poor for high forest cover areas. Analysis of the colour aerial imagery resulted in Fc computed from red ($mean = 0.95$, $coefficient\ of\ variation = 5.3\%$),

green (*mean* = 0.95, *coefficient of variation* = 4.8%) and blue (*mean* = 0.65, *coefficient of variation* = 13.63%) weekly associated with the measured *Fc* (*mean* = 0.88, *coefficient of variation* = 7.9%). No correlation was observed between measured and estimated *Fc* (Figure 2, $p > 0.01$, $n = 54$). *Fc* from red (*range*: 0.74-0.999) and green (*range*: 0.77-0.999) were considerably higher than that of blue (*range*: 0.5-0.863) and measured (*range*: 0.63-0.985) values.

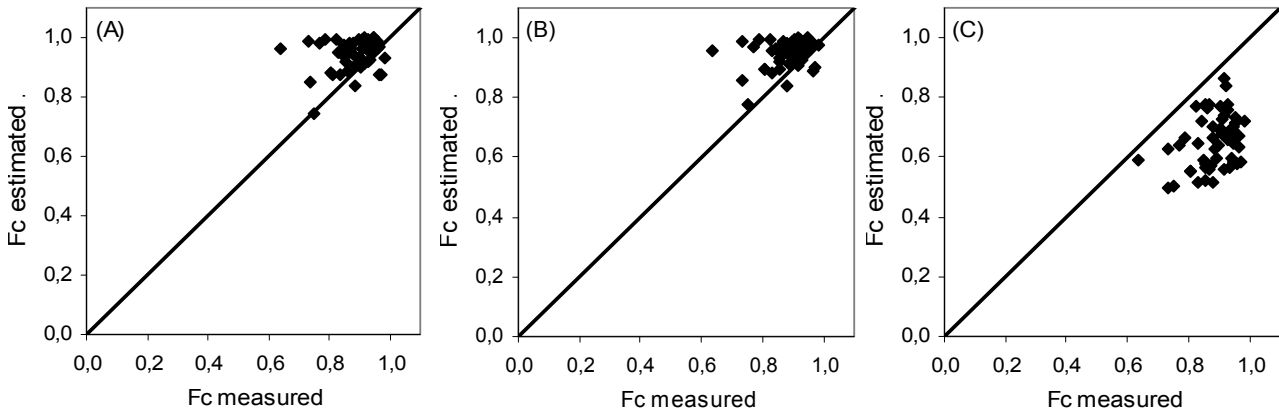


Figure 2: Relationships of measured and estimated fractional vegetation cover (*Fc*) computed from red (A), green (B), and blue (C) bands of colour image. Solid diagonal line represents a 1:1 relationship.

Similar to the poor correlation obtained between measured and estimated *Fc* using colour imagery, *LAI* estimates are also not correlated with measured values (Figure 3). *LAI* effective estimated using red and green bands is considerably higher than that of measured and estimated using the blue band. *LAI* effective estimated from red (*mean* = 6.8) was 68.5% higher, from green (*mean* = 7) was 74.7% higher and from blue (*mean* = 2.2) was 45.7% lower compared to measured *LAI* effective. The *Fc* and *LAI* estimated using the red and blue bands were highly correlated ($R^2 = 0.96$) (Figures 2 and 3). It can be concluded from Figures 2 and 3 that the colour image analysis was not feasible for gap fraction extraction and subsequently for *LAI* inversion in our dataset.

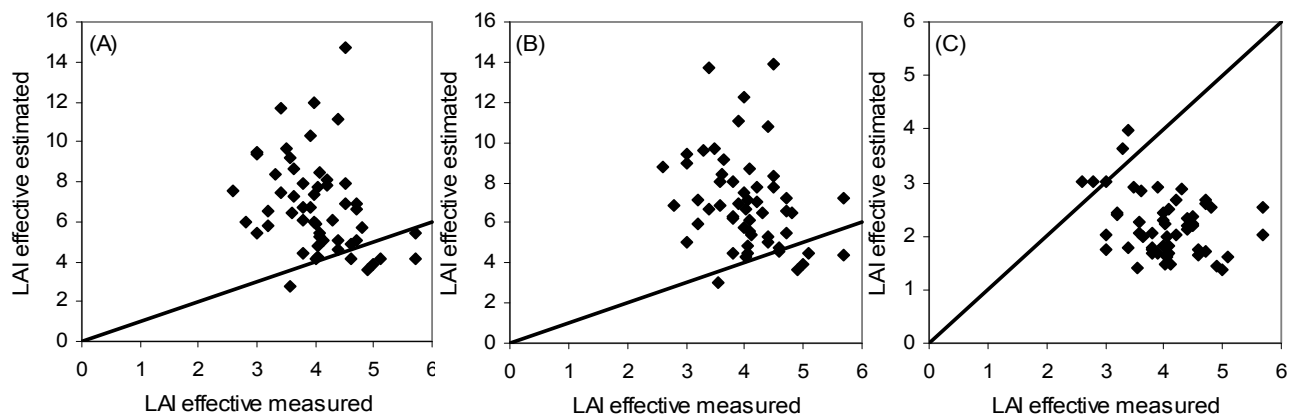


Figure 3: Relationships of measured and estimated *LAI* effective computed from red (A), green (B), and blue (C) bands of colour image. Solid diagonal line represents a 1:1 relationship.

The significant positive correlations (*Pearson correlation coefficient*: $R > 0.5$) observed between the measured and the estimated *LAI* through *NDVI* analysis of *CIR* image show great association between *LAI* and *NDVI* (Figures 4A, 4B and 4C). *LAI* effective from *NDVI* analysis resulted in a mean value of 4.3 compared to the measured *LAI* effective value of 4. However, the range (3.3-5.1) of estimated *LAI* effective from *NDVI* analysis is smaller than that of the measured range (2.6-5.7). The *NDVI* analysis resulted in greater *LAI* effective than the measured values for lower *LAI*s, and vice versa (Figure 4A). Thus we hypothesise that the understorey in lower *LAI* areas caused

the overestimation by significantly contributing to overall plot-wise *NDVI* compared to measured canopy *LAI* and *NDVI* tends to saturate in higher *LAI* plots.

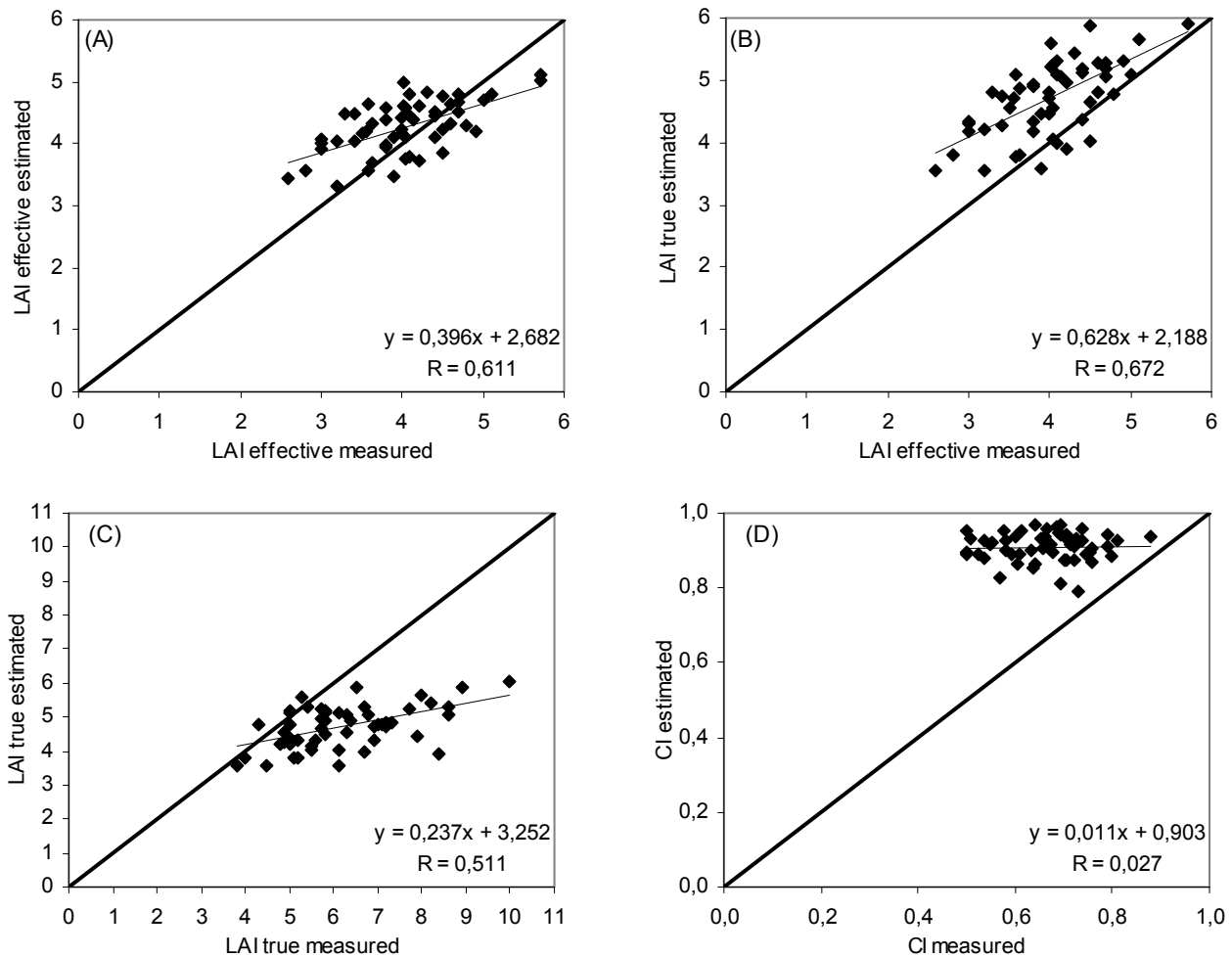


Figure 4: Relationships of measured and estimated *LAI* and clumping index (*CI*) computed from colour infrared image: (A) (*RMSE* = 0.342) between measured and estimated *LAI* effective, (B) (*RMSE* = 0.463) between measured *LAI* effective and estimated *LAI* true, (C) (*RMSE* = 0.537) between measured and estimated *LAI* true, and (D) (*RMSE* = 0.039, $p > 0.01$) between measured and estimated *CI*. Solid diagonal line represents a 1:1 relationship.

The clumping index was used as a correction parameter, particularly for ground measured *LAI* which otherwise underestimates true *LAI* values. However, this parameter is not particularly sensitive to changes within the same forest canopy types. We computed the *CI* from *NDVI* derived gap fraction with the same method used to compute it from hemispherical photography. The estimated *CI* is not correlated with the measured one (Figure 4D). However, the range obtained from *NDVI* analysis is in the order of realistic values for broadleaved canopies. Comparison between *LAI* effective, *LAI* true and *CI* derived from *NDVI* analysis from *CIR* images with corresponding measured values from ground measurement was carried out by performing regression and the results are presented in Figure 4B, 4C and 4D. Figure 4B shows that the estimated *LAI* true is the best correlated with measured *LAI* effective ($R = 0.67$). This indicates that the *CI* estimated from *NDVI* is a meaningful physical parameter for correction of *LAI* even though this kind of *CI* estimation does not exist in literature. The *LAI* true measured and estimated are positively correlated ($R = 0.5$) and the only underestimation from *NDVI* analysis in higher *LAI* values can be attributed to the possible saturation of *NDVI*. In general, *LAI* estimation from *CIR* imagery through *NDVI* analysis outperformed that of the colour imagery analysis even though the pixel size in colour images are relatively smaller than *CIR* images, giving the expectation of better performance for gap extraction. We hypothesise from these results that mass reflectance obtained in the *NIR* spectral region is more

important than the high resolution colour images to explain the forest cover density in multi-storey forest, as in the case of this study.

DISCUSSION AND CONCLUSIONS

In this paper, we investigated the feasibility of large-scale *LAI* inversion algorithms from high-resolution airborne imagery. The methodology demonstrated here is in line with the commonly used light extinction models for the determination of the probability of radiation interception within the layers of forest canopy and subsequently deriving key canopy biophysical parameters (14,23,24,25,26). The only difference here is that the canopy is observed from above to derive the mono-directional gap fraction. This is valid for two reasons: (a) the high-resolution imagery provides capability to distinguish gap from canopy, and (b) ground measured *LAI* and other canopy biophysical parameters are assumed to be empirically related with different reflectance factors and vegetation indices derived from top-of-canopy measurements.

The colour image generally produced poor results. Even though there is no study to compare with which attempted to estimate *LAI* directly from aerial colour images, the trend for fractional cover estimates from colour images is generally poor in dense vegetation zones. Some studies however successfully used high-resolution aerial colour images for tree crown delineation (27) and vegetation detection (28) in sparsely vegetated areas. The poor result of the thresholding approach from the colour image for fractional cover and *LAI* estimation might be explained by the denseness of the forest (*Fc* from ground measurement > 0.64) which is also illustrated in the low correlation of ground based and estimated *Fc* (Figure 2).

The use of fine resolution, colour infrared imagery showed promise as an accurate and relatively precise tool for large scale *LAI* inversion in a temperate hardwood forest in Gatineau Park. Our results indicated that the use of *NDVI* for *Fc*, gap fraction extraction and *LAI* inversion from *CIR* image was effective in relatively dense forest plots. Our result is relatively better compared to other works of *NDVI* analysis for *Fc* and *LAI* inversion, which were mainly conducted on low *LAI* areas (4,5,6,7,8,21,22). We also performed a sensitivity analysis by applying an exponential term computed by previous studies as a correction parameter for the retrieved gap fraction and *Fc* from *NDVI*, i.e.

$$\left(\frac{NDVI_g - NDVI}{NDVI_g - NDVI_{back}} \right)^{0.6157}$$

derived by a semi-empirical relationship between vertical gap and *NDVI* (21), and

$$\left(\frac{NDVI - NDVI_{back}}{NDVI_g - NDVI_{back}} \right)^2$$

derived based on a radiative transfer model (29). The retrieved *LAI* by applying the two exponential terms slightly underperformed compared to the relationship obtained between *LAI* derived from *Fc* without an exponential term and measured *LAI*.

The computation of clumping index from *NDVI* further improved the correlation of estimated and measured *LAI*. The assumption of logarithmic gap averaging technique for *CI* computation is more or less valid as long as gap sizes are concerned, which is obtained from *NDVI* (14). The gap size from gap fraction derived from *NDVI* can be interpreted as the possible dynamic range of the *NDVI* with regard to the individual pixel size. Compared to the previous attempts to compute *CI* directly from remotely sensed images (30,31), the method applied in this study has more practical and physical meaning for the correction of the obtained *LAI*.

Many existing methods of *LAI* estimation from remote sensing imagery usually require ground calibration data. A new *LAI* inversion methodology is demonstrated in this study. Compared with existing approaches, it not only has the advantage of the use of vegetation index models, it is easy and simple to use. We anticipate that with more accurate retrieval of saturated and background *NDVI* values, and further evaluation of the algorithms developed in this study, the methodologies to retrieve *LAI* and *CI* will lead to easy and effective utilisation of spectral information of remote sensing for vegetation studies.

ACKNOWLEDGEMENTS

The research was funded by the Academy of Finland through the TAITATOO-project and a personal grant to Petri Pellikka, and by Natural Sciences and Engineering Research Council of Canada funding to Douglas King. The first author is financed partly by CIMO, Department of Geography of University of Helsinki, and the Finnish Graduate School of Geography.

REFERENCES

- 1 Asner G P, J M O Scurlock & J A Hicke, 2003. Global synthesis of leaf area index observations: Implications for ecological and remote sensing studies. Global Ecology and Biogeography, 12: 191-205
- 2 Gonsamo A & P Pellikka, 2008. Methodology comparison for slope correction in canopy leaf area index estimation using hemispherical photography. Forest Ecology and Management, 256: 749-759
- 3 Chen J M & J Cihlar, 1996. Retrieving leaf area index of boreal conifer forests using Landsat TM images. Remote Sensing of Environment, 55: 153-162
- 4 Gutman A & G Ignatov, 1998. The Derivation of the Green Vegetation Fraction from NOAA/AVHRR Data for Use in Numerical Weather Prediction Models. International Journal of Remote Sensing, 19: 1533-1543
- 5 Sprintsin M, A Karnieli, P Berliner, E Rotenberg, D Yakir & S Cohen, 2007. The effect of spatial resolution on the accuracy of leaf area index estimation for a forest planted in the desert transition zone. Remote Sensing of Environment, 109: 416-428
- 6 Xiao J & A Moody, 2005. A comparison of methods for estimating fractional green vegetation cover within a desert-to-upland transition zone in central New Mexico, USA. Remote Sensing of Environment, 98: 237-250
- 7 Tang S, J M Chen, Q Zhu, X Li, M Chen, R Sun, Y Zhou, F Deng & D Xie, 2007. LAI inversion algorithm based on directional reflectance kernels. Journal of Environmental Management, 85: 638-648
- 8 Richardson A J & C L Wiegand, 1977. Distinguishing vegetation from soil background information. Photogrammetric Engineering and Remote Sensing, 43: 1541-1552
- 9 Hu B, J R Miller, J M Chen & A Hollinger, 2004. Retrieval of the canopy leaf area index in the BOREAS flux tower sites using linear spectral mixture analysis. Remote Sensing of Environment, 89: 176-188
- 10 Wulder M A, S E Franklin, & M B Lavigne, 1996. High spatial resolution optical image texture for improved estimation of forest stand leaf area index. Canadian Journal of Remote Sensing, 22: 441-449
- 11 Jonckheere I, S Fleck, K Nackaerts, B Muysa, P Coppin, M Weiss & F Baret, 2004. Review of methods for *in situ* leaf area index determination Part I. Theories, sensors and hemispherical photography. Agricultural and Forest Meteorology, 121: 19-35
- 12 Pellikka P, E D Seed & D J King, 2000. Modelling deciduous forest ice storm damage using aerial CIR imagery and hemispheric photography. Canadian Journal of Remote Sensing, 26: 394-405
- 13 Demarez V, S Duthoit, F Baret, M Weiss & G Dedieu, 2008. Estimation of leaf area and clumping indexes of crops with hemispherical photographs. Agricultural and Forest Meteorology, 148: 644-655
- 14 Lang A R G & Y Xiang, 1986. Estimation of leaf area index from transmission of direct sunlight in discontinuous canopies. Agricultural and Forest Meteorology, 35: 229-243
- 15 Pellikka P, 1998. Development of correction chain for multispectral airborne video camera data for natural resource assessment. Fennia, 176: 1-110

- 16 Lévesque J & D J King, 1999. Airborne Digital Camera Image Semivariance for Evaluation of Forest Structural Damage at an Acid Mine Site. Remote Sensing of Environment, 68: 112–124
- 17 Pellikka P, D J King & S G Leblanc, 2000. Quantification and reduction of bidirectional effects in deciduous forest in aerial *CIR* imagery using two reference land surface types. Remote Sensing Reviews, 19: 259-291
- 18 Pettorelli N, J O Vik, A Mysterud, J-M Gaillard, C J Tucker & N C Stenseth, 2005. Using the satellite-derived *NDVI* to assess ecological responses to environmental change. Trends in Ecology & Evolution, 20 (9): 503-510
- 19 Jiang Z, A R Huete, J Chen, Y Chen, J Li, G Yan & X Zhang, 2007. Analysis of *NDVI* and scaled difference vegetation index retrievals of vegetation fraction. Remote Sensing of Environment, 101: 366-378
- 20 Carpenter G A, S Gopal, S Macomber, S Martens & C E Woodcock, 1999. A neural network method for mixture estimation for vegetation mapping. Remote Sensing of Environment, 70: 138-152
- 21 Baret F, J G P W Clevers & M D Steven, 1995. The robustness of canopy gap fraction estimates from red and near-infrared reflectances: a comparison of approaches. Remote Sensing of Environment, 54: 141–151
- 22 Zeng X, R E Dickinson, A Walker, M Shaikh, R S DeFries & J Qi, 2000. Derivation and evaluation of global 1-km fractional vegetation cover data for land modelling. Journal of Applied Meteorology, 39: 826–839
- 23 Bréda N J J, 2003. Ground-based measurements of leaf area index: a review of methods, instruments and current controversies. Journal of Experimental Botany, 54: 2403–2417
- 24 Nilson T, 1971. A theoretical analysis of the frequency of gaps in plant stands. Agricultural and Forest Meteorology, 8: 25–38
- 25 Miller J B, 1967. A formula for average foliage density. Australian Journal of Botany, 15: 141-144
- 26 Ross J, 1981. The radiation regime and architecture of plant stands (Dr Junk Publishers) 392 pp.
- 27 Wang L, P Gong & G S Biging, 2004. Individual Tree-Crown Delineation and Treetop Detection in High-Spatial-Resolution Aerial Imagery. Photogrammetric Engineering and Remote Sensing, 70: 351-357
- 28 Chen L-C, T-A Teo & T-W Chiang, 2006. The Generation of 3D Tree Models by the Integration of Multi-sensor Data. In: Advances in Image and Video Technology (Springer, Berlin, Heidelberg) pp. 34-43
- 29 Carlson T N & D A Ripley, 1997. On the relation between *NDVI*, fractional vegetation cover, and leaf area index. Remote Sensing of Environment, 62: 241-252
- 30 Chen J M, C H Menges & S G Leblanc, 2005. Global mapping of foliage clumping index using multi-angular satellite data. Remote Sensing of Environment, 97: 447-457
- 31 Lacaze R, J M Chen, J-L Roujean & S G Leblanc, 2002. Retrieval of vegetation clumping index using hot spot signatures measured by POLDER instrument. Remote Sensing of Environment, 79: 84-95